Arch. Metall. Mater. **71** (2026), 3, 737-749

DOI: https://doi.org/10.24425/amm.2026.1963

IZABELLA KWIECIEN[1], MARTA JANUSZ-SKUZA[1], AGNIESZKA BIGOS[1], MONIKA BUGAJSKA[1], ANNA WIERZBICKA-MIERNIK[1], SOFIA GAMBARO[2], FABRIZIO VALENZA[2], JOANNA WOJEWODA-BUDKA[1*]

MODERN RHENIUM-MODIFIED Ni-P SURFACE FINISHES: WETTING AND INTERFACIAL REACTIONS WITH Sn-3.0Ag-0.5Cu SOLDER UNDER THERMAL CYCLING SIMULATION

The transition to lead-free soldering technology has driven significant research into advanced finishing layers with improved thermal stability and controlled interfacial reactivity. ENIG PCB finish is widely used in electronics, particularly in surface-mount technology for printed circuit boards. In the present work, previous studies on the reactivity of electroless Ni-P-Re finishing layers with varying phosphorus content were continued, this time using commercially available SAC305 solder (Sn-3.0Ag-0.5Cu). The addition of rhenium is expected to suppress or eliminate the massive detachment of intermetallic phases from the interface and their migration into the solder. To this end, three surface finish variants with different phosphorus content but constant rhenium content were deposited. The wettability of both Ni-P and Ni-P-Re finishing layers with SAC305 alloy was investigated using the sessile drop method. The obtained systems were subsequently subjected to cyclic heating and cooling to simulate typical operating conditions of electronic devices. The finishing layers, as well as the surface finish/solder systems before and after thermal cycling, were characterized using scanning and transmission electron microscopy together with energy-dispersive X-ray spectroscopy to evaluate microstructural and compositional changes. The results revealed a significant influence of both phosphorus content and rhenium addition on the sequence of interfacial phase formation and on the fraction of $(Cu,Ni)_6Sn_5$ phase spalling into the solder volume. The presence of both elements strongly affected the formation and thickness of the undesirable Ni_2SnP phase at the interface, both immediately after the wetting test and after thermal cycling.

Keywords: Ni-P finishing layers; ENIG; Electroless deposition; Rhenium; Interfacial reactivity

1. Introduction

Electroless Ni-P finishing layers are widely used in the electronics industry, particularly in surface-mount technology (SMT) for printed circuit boards (PCBs). In industrial applications, these surface finishes are commonly known as Electroless Nickel Immersion Gold (ENIG) systems, in which a thin top layer of gold either electroplated (0.6-0.7 μm) or deposited by immersion (0.1-0.15 μm) is applied to improve wettability, while the underlying nickel layer acts as a barrier to prevent copper diffusion [1]. The introduction of the European Union directive 2002/95/EC, restricting the use of hazardous substances such as Pb in electronic applications [2], has driven significant research efforts toward the study of new-generation Pb-free solders [3] as well as surface finishes with improved physical and chemical properties [4-9]. One of the key challenges is the requirement for enhanced thermal stability of nickel-based finishing layers, along with control the growth of intermetallic compounds (IMCs) at the surface finish/solder interface. Ideally, a thin and continuous intermetallic layer should form at the interface. However, excessive growth, detachment, and migration of intermetallic phases into the solder can lead to mechanical degradation and eventual failure of the interconnection. Due to the low cost and favorable properties, such as high mechanical strength and good thermal fatigue resistance, one of the most commonly used Pb-free solders is SAC305 [10]. A significant drawback of this alloy is its higher processing (soldering) temperature and increased reactivity, which promotes the formation of more extensive intermetallic phases at the interface compared to conventional Sn-Pb solders [11]. The application of new-generation solders such as SAC305 is associated with increased joining temperatures, thereby creating a need for the development of advanced diffusion barrier finishing layers. A promising approach to improving the thermal stability of nickel finishing layers is the incorporation

[1] INSTITUTE OF METALLURGY AND MATERIALS SCIENCE, POLISH ACADEMY OF SCIENCES, 25 W. REYMONTA STR., 30-059 KRAKOW, POLAND
[2] INSTITUTE OF CONDENSED MATTER CHEMISTRY AND TECHNOLOGIES FOR ENERGY, NATIONAL RESEARCH COUNCIL, GENOA, ITALY

* Corresponding author: j.wojewoda@imim.pl

of additional elements into their structure, such as tungsten [12], molybdenum [4-5], rhenium [6-7], or cobalt [13]. Studies have shown that the addition of rhenium to electroless Ni-P finishing layers may suppress the formation of the Ni_2SnP phase, which contributes to the massive detachment of intermetallic compounds from the interface. Molybdenum in electrodeposited Ni finishing layers hinders diffusion between the substrate and the solder, while alloying Ni-P finishing layers with elements such as Co and W enhances the durability and long-term reliability of solder joints.

The present study is focused on the modification of Ni-P finishing layers through the addition of rhenium, with the aim of improving their reliability after thermal cycling and mitigating the spalling of intermetallic compounds. This work continues previous investigations on Ni-P and Ni-P-Re finishing layers, extending the research to phenomena occurring at the interface between Ni-P and Ni-P-Re finishing layers and the conventional SAC305 solder alloy. It is expected that the addition of rhenium may retard or eliminate formation of unfavorable Ni_2SnP phase correlated with the massive detachment of intermetallic phases from the interface into the solder during interaction at elevated temperature. In this study, Ni-P and Ni-P-Re finishing layers with varying phosphorus content (low, medium, and high) were deposited from an acidic hypophosphite bath. The surface morphology and topography of the finishing layers, their chemical composition, wetting behavior, and reactivity with liquid SAC305 alloy using the sessile drop method were intensively investigated. The surface finish/solder interfaces were examined by scanning and transmission electron microscopy, with particular emphasis on assessing the quality of the interface zone and identifying the intermetallic phases formed. Furthermore, thermal cycling was applied to simulate standard operating conditions in electronic systems in order to investigate the effect of cyclic temperature variations on the previously formed interfaces.

2. Material and methods

All finishing layers were produced from aqueous plating solutions on copper substrates. Prior to the deposition process, copper substrates were etched in a 1:1:1 mixture of nitric, acetic, and phosphoric acids, and then thoroughly rinsed with deionized water. The chemical compositions of the electroless baths, along with the corresponding operating parameters, are summarized in TABLE 1. Deionized water (18.2 MΩ·cm^{-1}) and analytical-grade reagents were used as the basis of the plating solutions. The finishing layers were deposited for 45 minutes at a temperature of 80 ± 5°C. By appropriately controlling the pH value of the bath and the concentration of ammonium perrhenate, a series of Ni-P-Re finishing layers was produced, corresponding in chemical composition to the reference Ni-P one. After deposition, the samples were carefully cleaned with deionized water and then ultrasonicated in ethanol for 5 minutes and dried. Subsequently, the samples were coated with a 2-3 nm thick gold layer by magnetron sputtering.

The wetting and interfacial interactions between liquid SAC305 and the ENIG finishing layers were investigated using the sessile drop method. The experiments were performed in a tubular quartz chamber heated by a high-frequency generator coupled with a vitreous carbon susceptor [14]. Initially, the surface finish/SAC305 couples were preheated to 100°C and subsequently heated at a rate of approximately 36°C/min up to the final test temperature of 280°C. After a holding time of 60 s, the samples were rapidly cooled by switching off the power. All tests were conducted under vacuum, maintained below 10^{-2} Pa throughout the experiment. Prior to testing, small pieces of SAC305 alloy (approximately 0.5 g; Sn: 96.5, Ag: 3.0, Cu: 0.5 wt.%; liquidus: 220°C; solidus: 217°C) were prepared from a single batch. The samples were pre-melted in an arc-melting device to obtain spherical and clean droplets. Subsequently, the droplets and the ENIG substrates were cleaned in an ultrasonic bath with alcohol to remove surface contaminants and ensure reproducible wetting conditions. The samples were weighed before and after the tests; the mass loss due to tin evaporation was below 1%. The images recorded during the experiments were analyzed using in-house developed software to accurately determine the contact angles.

Following wetting, the samples were subjected to repeated heating and cooling cycles to simulate thermal shocks during standard electronic device operation (Fig. 1).

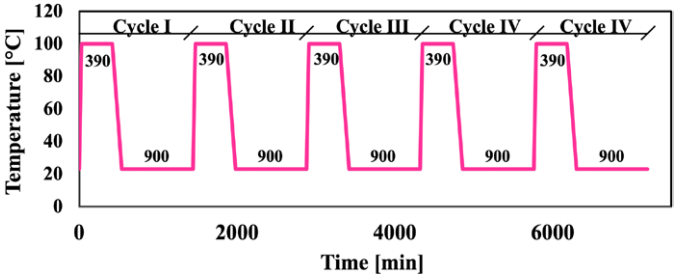

Fig. 1. Temperature profile simulating thermal shocks during standard device operation

Microstructural observations of the surface finish surfaces and surface finish/solder cross-sections were performed using a scanning electron microscope (SEM, FEI E-SEM XL30) equipped with a tungsten filament. The microscope was equipped with an energy-dispersive X-ray spectrometer (EDS, EDAX

TABLE 1

The chemical composition of the electroless Ni-P and Ni-P-Re baths and the plating process parameters

Sample	Bath Composition [M]	NH_4ReO_4 [M]	pH	Temperature [°C]
Ni-P3.8	$NiSO_4 \cdot 7H_2O$ – 0.100 $NaH_2PO_4 \cdot H_2O$ – 0.200 $Na_2C_4H_4O_4 \cdot 6H_2O$ – 0.400	—	3.8	80 ± 5
Ni-P4.8		—	4.8	
Ni-P5.6		—	5.6	
Ni-P-Re3.6		0.0025	3.6	
Ni-P-Re4.7		0.0015	4.7	
Ni-P-Re5.5		0.0020	5.5	

Gemini) applied for chemical composition analysis of all samples. Thin foils were prepared using the focused ion beam (FIB) technique with a SEM Thermo Fisher Scientific SCIOS 2 Dual Beam system (field emission gun). The prepared specimens were then analyzed by transmission electron microscopy (TEM, Tecnai G2 FEI).

3. Results and discussion

3.1. Ni-P and Ni-P-Re finishing layers characterization

All deposited finishing layers are characterized by a morphology typical of electroless nickel, as reported in the literature (see [15-16]). Finishing layers exhibited a matt silver-colored surface. SEM/SE observations (Fig. 2a-f) revealed a homogeneous, compact structure free of defects such as cracks and porosity. The characteristic nodular morphology, composed of many small grains, differed depending on the process conditions. The term "grain" in surface morphology does not refer to individual crystals, but rather to granular particles formed during the deposition process, consisting of much smaller crystals or even an amorphous structure [16]. The addition of ammonium perrhenate to the electroless bath did not significantly affect the surface morphology. The most important parameter, which determines not only the surface morphology but also the process efficiency, surface finish crystallographic structure, and the concentration of P and Re within the finishing layers, is the bath pH (assuming a constant process temperature [16-17]).

The surface topography of the Ni-P and Ni-P-Re finishing layers is presented in Fig. 3 in the form of 3D surface profiles obtained by confocal microscopy. For the Ni-P finishing layers (Fig. 3a-c), the surface nodular morphology exhibited a relatively uniform distribution of asperities. The roughness parameter Sa varies between approximately 0.43 and 0.65 µm, with the highest roughness observed for the surface finish deposited at pH = 4.8. In contrast, the Ni-P-Re finishing layers (Fig. 3d-f) show a slightly more refined and homogeneous surface morphology, although local heterogeneities are still present. The Sa values range from approximately 0.45 to 0.62 µm, indicating comparable but slightly lower or more uniform roughness compared to the Ni-P finishing layers. In particular, the finishing layers deposited at intermediate pH exhibit a more uniform distribution of surface features. Ni-P3.8 and Ni-P-Re3.6 are characterized by the smallest grains and the least developed surface morphology, as well as the lowest roughness (Sa = 0.43 µm and 0.45 µm, respectively; see Fig. 3a,d). In the case of the intermediate pH value, for Ni-P4.8 and Ni-P-Re4.7, the grains were larger and the roughness reached the highest values (Sa = 0.65 µm and 0.62 µm, respectively; see Fig. 3b,e). For Ni-P5.6 and Ni-P-Re5.5, the grain size and roughness were intermediate (Sa = 0.57 µm and 0.46 µm, respectively; see Fig. 3c,f). Such changes in morphology can be related to the process efficiency, defined as the deposition rate. Kazimierczak et al. [16] reported an increase in process efficiency with increasing pH of the electroless solution, while in the pH range of 4.0-5.5 the efficiency of the Ni-P-Re series was slightly lower than that of the Ni-P series (see Fig. 1b in Kazimierczak [16]). Within this range, the maximum efficiency occurred at pH = 5.0. The pH ranges given were consistent with the pH range reported in this paper. The maximum finishing layers thickness (being a measure of the effectiveness of the process) was observed for Ni-P4.8 – 11 µm and Ni-P-Re4.7 – 7 µm. Lower values were obtained below this pH, for Ni-P3.8 – 3 µm and Ni-P-Re3.6 –1 µm, and above this pH, for Ni-P5.6 – 6 µm and Ni-P-Re5.5 – 3 µm. These results confirm the same tendency of process efficiency changes with pH and the presence of ammonium perrhenate in the bath in the current study as that reported by Kazimierczak et al. [16].

Control of process parameters such as pH and ammonium perrhenate concentration enabled the preparation of a series of Ni-P-Re finishing layers in three variants differing in phosphorus content, while maintaining the rhenium content at a similar

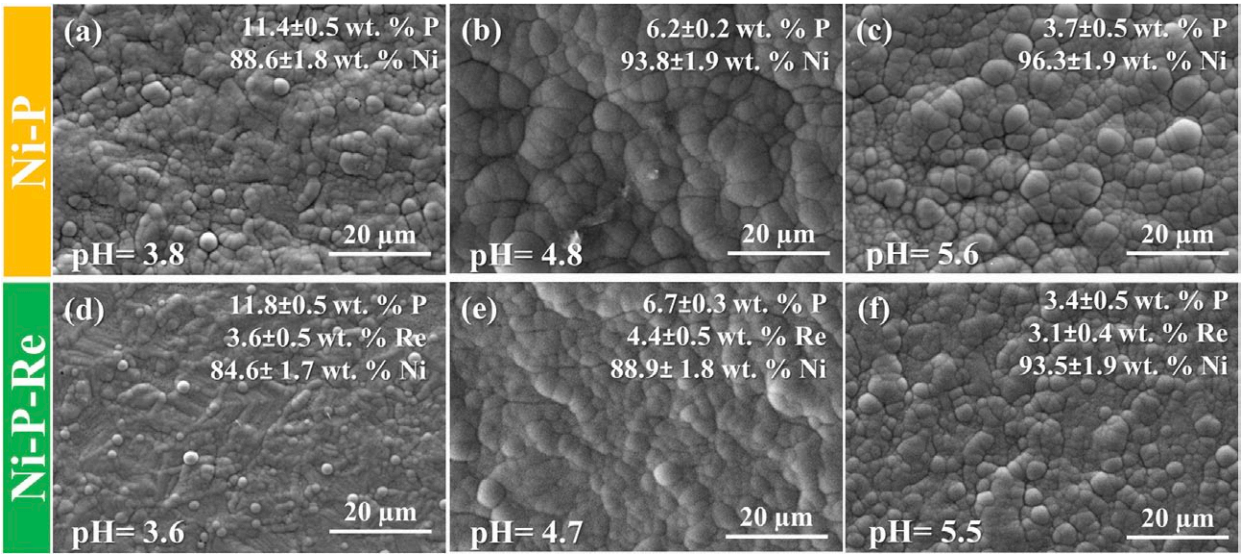

Fig. 2. Surface morphology of the Ni-P (a-c) and Ni-P-Re (d-f) finishing layers plated on copper at different bath pH conditions

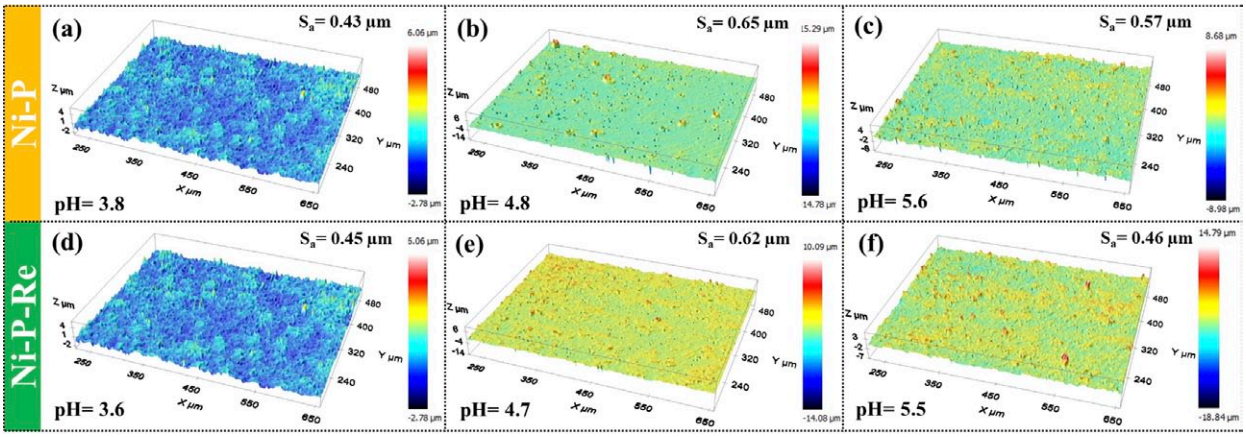

Fig. 3. 3D surface topography profiles of the Ni-P (a-c) and Ni-P-Re (d-f)

level of 3-4 wt.%. Additionally, a reference series of Ni-P finishing layers with the same phosphorus levels was prepared. The phosphorus content in the Ni-P finishing layers determines their crystallographic structure, which may be amorphous (high phosphorus content), a mixture of amorphous and nanocrystalline (medium phosphorus content), or nanocrystalline (low phosphorus content) [15,17]. Based on our previous experience [17] and literature data [15], the studied finishing layers were designed to obtain each of these structural variants. The full chemical composition for each surface finish was added to Fig. 2.

3.2. Wetting and interfacial reactivity of Ni-P and Ni-P-Re finishing layers with SAC305

The wetting behavior of liquid SAC305 on Ni-P and Ni-P-Re finishing layers, evaluated by the sessile drop method, is presented in Fig. 4. Representative CCD images of the droplets during testing, along with selected post-test views of the samples, are shown for different bath pH values. It should be noted that the measured contact angles may be influenced by pinning effects at the triple line induced by surface asperities (Fig. 3) which can locally hinder the motion of the contact line. As a result, the measured contact angles may deviate from their equilibrium values, contributing to the observed scatter. For the Ni-P finishing layers (Fig. 4a-c), the measured contact angles exhibit moderate wettability, with values ranging from approximately 42-63°. The Ni-P-Re finishing layers (Fig. 4d-f) show consistently lower contact angles, in the range of approximately 27-40°, indicating enhanced wettability compared to the Ni-P counterparts. The lowest values were recorded for the finishing layers deposited at higher pH (pH = 5.5), where contact angles decreased to about 27-29°, corresponding to improved spreading behavior of the SAC305 alloy. The comparison between the two surface finish systems demonstrates that the addition of rhenium leads to an improvement of the wetting performance.

The differences in wettability can be related to the interfacial reactions occurring during the tests. The SEM/BSE cross-

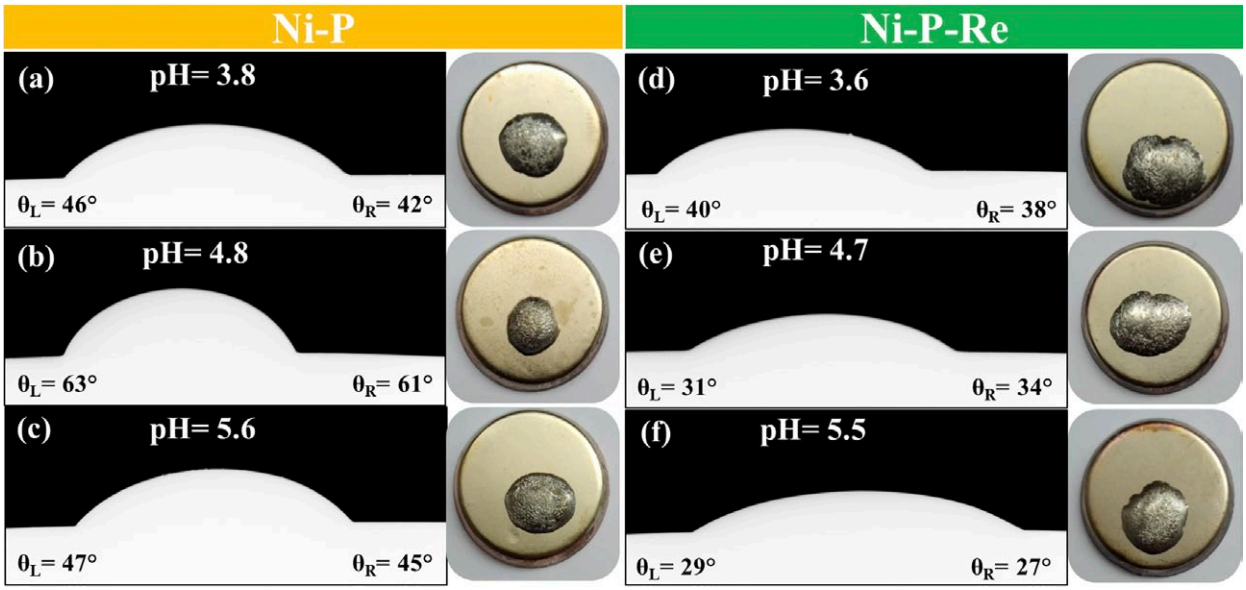

Fig. 4. CCD camera images recorded during sessile drop tests of liquid SAC305 drops on Ni-P (a-c) and Ni-P-Re (d-f) finishing layers (left) and an exemplary sample after wetting tests (right)

sectional images of the Ni-P/SAC305 and Ni-P-Re/SAC305 interfaces formed after the sessile drop tests are presented in Fig. 5. The average chemical compositions determined for regions 1-8 marked in Fig. 5a-d were listed in TABLE 2. In both the Ni-P/SAC305 and Ni-P-Re/SAC305 couples, a layered arrangement of intermetallic phases formed along the interfaces, with a growth amount of scallop-type intermetallic phases observed on the side facing the SAC305 solder. For the Ni-P finishing layers, a continuous reaction layer was observed in all cases, although its internal structure depended on the deposition pH. The interaction between the solder and the finishing layers strongly depended on the phosphorus content. For high-phosphorus Ni-P and Ni-P-Re layers, intense detachment and migration of the scallop-type phase toward the bulk solder were observed. The spalling phenomenon was gradually eliminated with decreasing phosphorus content. In [7], the authors indicated that the addition of up to 1 wt.% rhenium to Ni-P layers may limit the massive detachment of intermetallic phases from the interface, which is correlated with the suppressed growth of the Ni_2SnP layer compared with Ni-P finishing layers. The formation of the unfavorable Ni_2SnP layer is a common problem in Ni-P finishing layers, particularly with a higher phosphorus content [6,7,18,19]. The mechanisms of Ni_2SnP phase formation were described in detail by Wojewoda-Budka in [6]. In the current study, the Ni-P3.8 (Fig. 5a) and Ni-P-Re3.6 (Fig. 5d) finishing layers contained a phosphorus content similar to that reported in [7]. However, in the present case, even the higher rhenium content (~4.0 wt.%) did not prevent the migration of intermetallics from the interface into the SAC305 solder. These differences are strongly correlated with the thickness of the Ni-P-Re3.6 coating, which was approximately 1 μm, whereas in [7] it was about 5 μm. In the case of the Ni-P3.8 sample, where surface finish was thicker (3.1 μm), the interface exhibited a layered structure. The distribution of chemical elements across the interface is presented in Fig. 6a as a line scan. Sharp compositional gradients were observed, with a clear transition from Ni-rich regions in the surface finish to Sn-rich regions in the solder, accompanied by Cu diffusion. The layer adjacent to the Cu substrate was depleted in Ni compared to the initial Ni-P3.8 surface finish and is referred to as the Ni-$P_{P\text{-}rich}$ layer (TABLE 2). Its formation is associated with the diffusion of Ni atoms into the SAC solder, while phosphorus accumulates at the interface. Typically, when the initial Ni-P layer is thicker, the surface finish undergoes segregation, and only the surface layer at the solder interface becomes depleted in Ni, whereas the remainder of the surface finish retains a composition similar to that of the original layer [12,20,21]. The next relatively thick (~0.8 μm) layer was determined as ternary Ni_2SnP phase and bulk $(Cu,Ni)_6Sn_5$ scallops. Large loosely

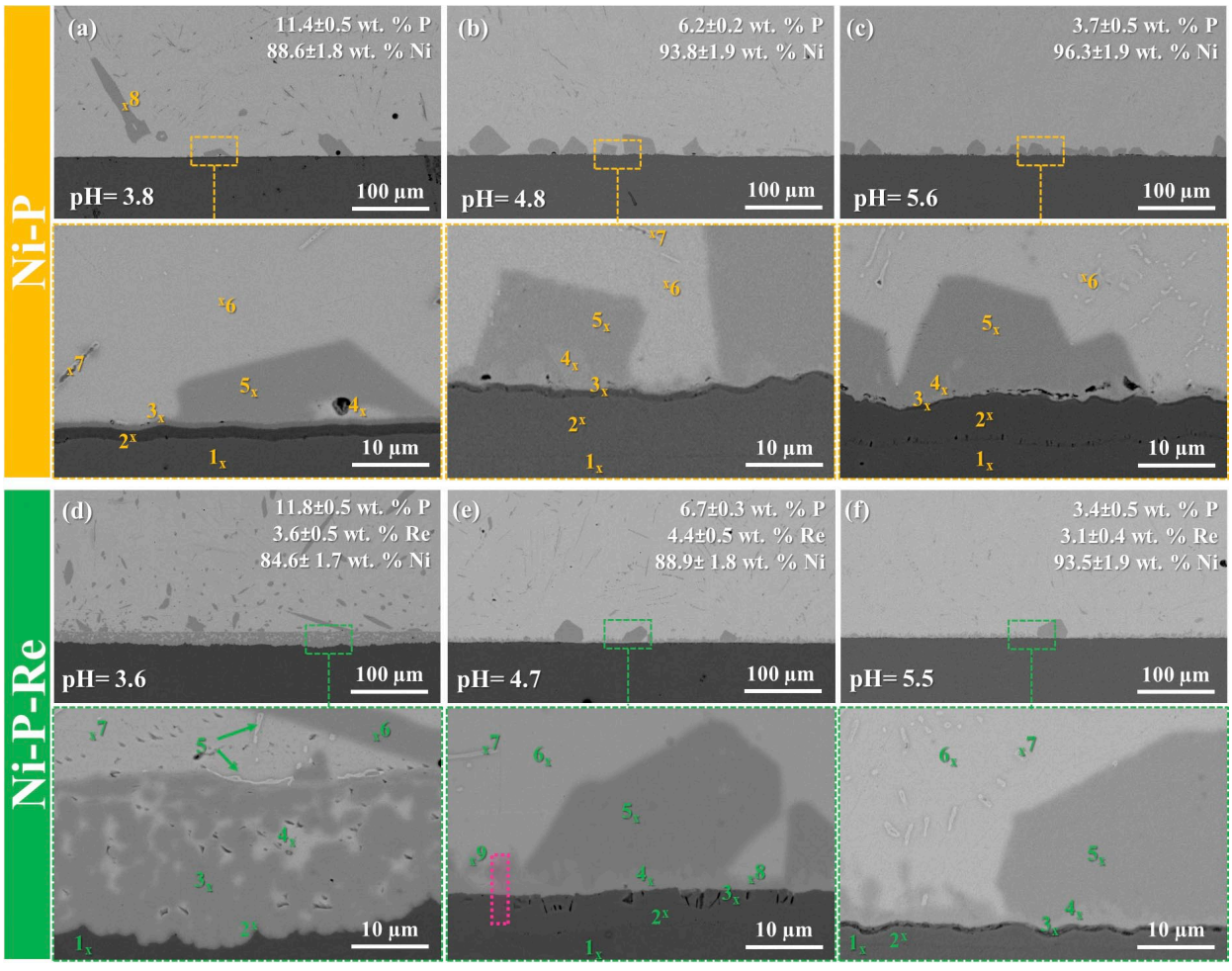

Fig. 5. SEM/BSE images of the interface cross sections Ni-P/SAC305 (a-c) and Ni-P-Re/SAC305 (d-f) after wetting test

TABLE 2

Average values of the SEM-EDS chemical composition collected from marked places of the cross sections Fig. 5a-f

Ni-P3.8 (Fig. 5a)																			
No	**Ni [at. %]**			**P [at. %]**			**Re [at. %]**			**Cu [at. %]**			**Sn [at. %]**			**Ag [at. %]**			**Possible Phase**
1		—			—			—		100.0	±	2.0		—			—		$Cu_{substrate}$
2	60.9	±	1.2	27.8	±	1.1		—		11.3	±	0.5		—			—		$Ni\text{-}P_{P\text{-}rich}$
3	54.6	±	1.1	26.2	±	1.0		—		3.2	±	0.5	16.0	±	0.7		—		Ni_2SnP
4	7.9	±	1.2		—			—		10.2	±	0.5	81.9	±	1.6		—		$Sn_{inclusion}$
5	18.8	±	0.8		—			—		37.9	±	0.8	43.3	±	0.9		—		$(Cu,Ni)_6Sn_5$
6		—			—			—			—		100.0	±	2.0		—		Sn
7		—			—			—			—		85.0	±	1.7	15.0	±	0.6	$Sn + Ag_3Sn$
8	18.4	±	0.7		—			—		37.3	±	0.7	44.3	±	0.9		—		$(Cu,Ni)_6Sn_5$
Ni-P4.8 (Fig. 5b)																			
No	**Ni [at. %]**			**P [at. %]**			**Re [at. %]**			**Cu [at. %]**			**Sn [at. %]**			**Ag [at. %]**			**Possible Phase**
1		—			—			—		100.0	±	2.0		—			—		$Cu_{substrate}$
2	91.3	±	1.8	8.7	±	0.9		—			—			—			—		Ni-P
3	78.1	±	1.6	21.1	±	0.8		—			—		0.8	±	0.6		—		$Ni\text{-}P_{P\text{-}rich}$
4	38.1	±	0.8		—			—		9.1	±	0.5	52.8	±	1.1		—		$(Ni,Cu)_3Sn_4$
5	21.6	±	0.9		—			—		35.1	±	0.7	43.3	±	0.9		—		$(Cu,Ni)_6Sn_5$
6		—			—			—			—		100.0	±	2.0		—		Sn
7		—			—			—			—		61.6	±	1.2	38.4	±	0.8	$Sn + Ag_3Sn$
Ni-P5.6 (Fig. 5c)																			
No	**Ni [at. %]**			**P [at. %]**			**Re [at. %]**			**Cu [at. %]**			**Sn [at. %]**			**Ag [at. %]**			**Possible Phase**
1		—			—			—		100.0	±	2.0		—			—		$Cu_{substrate}$
2	93.7	±	1.9	6.3	±	0.9		—			—			—			—		Ni-P
3	93.8	±	1.9	6.2	±	0.9		—			—			—			—		$Ni\text{-}P_{P\text{-}rich}$ (see Fig. 6c)
4	22.7	±	0.5		—			—		33.7	±	0.7	43.6	±	0.9		—		$(Ni,Cu)_3Sn_4$ (see Fig. 6c)
5	26.0	±	1.0		—			—		28.2	±	0.6	45.8	±	0.9		—		$(Cu,Ni)_6Sn_5$
6					—			—			—		94.4	±	1.9	5.6	±	0.8	$Sn + Ag_3Sn$
Ni-P-Re3.6 (Fig. 5d)																			
No	**Ni [at. %]**			**P [at. %]**			**Re [at. %]**			**Cu [at. %]**			**Sn [at. %]**			**Ag [at. %]**			**Possible Phase**
1		—			—			—		100.0	±	2.0		—			—		$Cu_{substrate}$
2		—			—			—		56.6	±	1.1	43.4	±	0.9		—		$(Cu,Ni)_6Sn_5$
3	8.2	±	0.5		—			—		44.7	±	0.9	47.1	±	0.9		—		$(Cu,Ni)_6Sn_5$
4		—			—			—		5.9	±	0.6	94.1	±	1.9		—		Sn
5		—			—			—			—		80.0	±	1.6	20.0	±	0.8	$Sn + Ag_3Sn$
6	9.8	±	0.5		—			—		45.3	±	0.9	44.9	±	0.9		—		$(Cu,Ni)_6Sn_5$
7	—				—			—			—		100.0	±	2.0		—		Sn
Ni-P-Re4.7 (Fig. 5e)																			
No	**Ni [at. %]**			**P [at. %]**			**Re [at. %]**			**Cu [at. %]**			**Sn [at. %]**			**Ag[at. %]**			**Possible Phase**
1		—			—			—		100.0	±	2.0		—			—		$Cu_{substrate}$
2	87.7	±	1.8	12.3	±	0.5		—			—			—			—		Ni-P-Re
3	67.4	±	1.3	27.6	±	1.1	3.5	±	0.1		—		1.5	±	0.8		—		$Ni\text{-}P\text{-}Re_{P,Re\text{-}rich}$
4	36.3	±	0.7		—			—		10.1	±	0.5	53.6	±	1.1		—		$(Ni,Cu)_3Sn_4$
5	20.9	±	0.8		—			—		34.3	±	0.7	44.8	±	0.9		—		$(Cu,Ni)_6Sn_5$
6		—			—			—			—		100.0	±	2.0		—		Sn
7		—			—			—			—		42.9	±	0.9	57.1	±	1.1	$Sn + Ag_3Sn$
8	33.0	±	0.7		—			—		10.2	±	0.4	56.8	±	1.1		—		$(Ni,Cu)_3Sn_4$
9	22.6	±	0.9		—			—		31.2	±	0.6	46.2	±	0.9		—		$(Cu,Ni)_6Sn_5$
Ni-P-Re5.5 (Fig. 5f)																			
No	**Ni [at. %]**			**P [at. %]**			**Re [at. %]**			**Cu [at. %]**			**Sn [at. %]**			**Ag [at. %]**			**Possible Phase**
1		—			—			—		100.0	±	2.0		—			—		$Cu_{substrate}$
2	93.9	±	1.9	5.5	±	0.8	0.6	±	0.6		—			—			—		Ni-P-Re
3	86.5	±	1.7	12.9	±	0.5		—			—		0.6	±	0.6		—		$Ni\text{-}P\text{-}Re_{P\text{-}rich}$
4	40.2	±	0.8	2.0	±	1.0		—		8.6	±	0.5	49.2	±	1.0		—		$(Ni,Cu)_3Sn_4$
5	21.5	±	0.9		—			—		35.4	±	0.7	43.1	±	0.9		—		$(Cu,Ni)_6Sn_5$
6		—			—			—			—		100.0	±	2.0		—		Sn
7		—			—			—			—		54.4	±	1.1	45.6	±	0.9	$Sn + Ag_3Sn$

arranged precipitates in the solder matrix were also identified as $(Cu,Ni)_6Sn_5$. In the case of the thin Ni-P-Re3.6 coating, that dissolved into the solder and formed a dispersed layer composed of small clusters of $(Cu,Ni)_6Sn_5$. Fig. 6d shows a slight peak indicating the presence of rhenium at the interface between the substrate and the dispersed layer. The decrease in phosphorus content within both the Ni-P and Ni-P-Re finishing layers below 7 wt.% eliminated the formation of the Ni_2SnP phase after contact with molten SAC305 solder during the wetting test. Part of the interface corresponding to the initial Ni-P4.8 (Fig. 5b) and Ni-P-Re4.7 (Fig. 5e) finishing layers was divided into a chemically unchanged region (compare to initial coating) on the copper substrate side and a region enriched in phosphorus and rhenium on the solder side (TABLE 2). Within these nickel-depleted regions, voids were formed, which were more pronounced in the Ni-P-Re4.7 sample. The formation of the voids is related to the fast diffusion of Ni atoms toward the solder. Such conditions favor the crystallization of the $(Ni,Cu)_3Sn_4$ phase at the boundary with the coating, inside the large scallops of $(Cu,Ni)_6Sn_5$. EDS line scans presented in Figs. 6b and 6e clearly demonstrate the

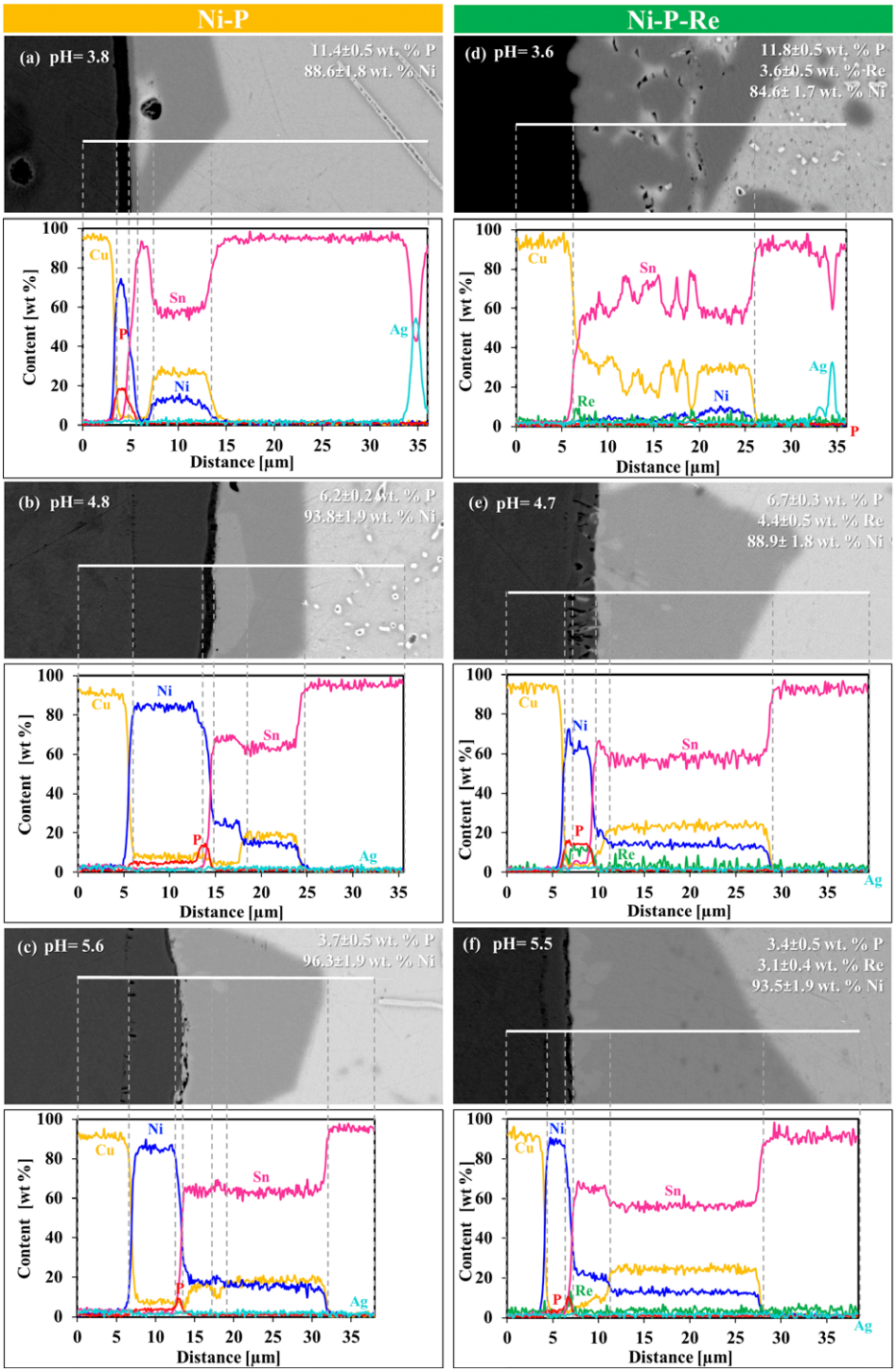

Fig. 6. SEM/BSE cross-sections of (a-c) Ni-P/SAC305 and (d-f) Ni-P-Re/SAC305 interfaces with corresponding EDS line scans for Ni, P, Re, Cu, Sn, and Ag concentrations

described changes in chemical composition across the cross-section, both on the surface finish and solder sides. A further decrease in phosphorus content within the Ni-P5.6 (Fig. 5c) and Ni-P-Re5.5 (Fig. 5f) samples below 4 wt.% did not affect the sequence of reaction products formed at the interface after contact with the liquid solder; however, in both cases, a narrowing of the regions enriched in phosphorus and rhenium was observed (Figs. 6c and 6f) from about 1 μm (Ni-P4.8) to 0.5 μm (Ni-P5.6) and 2 μm (Ni-P-Re4.7) to 1 μm (Ni-P-Re5.5). In contrast to Ni-P finishing layers, the Ni-P-Re finishing layers exhibited smoother compositional gradients and thinner reaction zones, indicating reduced interdiffusion. Rhenium was detected within the surface finish but showed no significant enrichment in the intermetallic phases, suggesting that its role is primarily related to modification of the surface finish matrix rather than direct participation in phase formation.

Bigos et al. [5] reported the formation of a continuous nanometric layer with a brighter SEM/BSE contrast at the phase boundary of the Ni-Mo/SAC305 coating, but the authors corelated that with accumulation of the molybdenum within this zone, rather than formation $(Cu,Ni)_6Sn_5$ or $(Ni,Cu)_3Sn_4$ phases at the interface. Moreover, the authors pointed that such zone may effectively suppressed diffusion of nickel into solder that slower growth of the intermetallic phases at interface. In the studied Ni-P and Ni-P-Re finishing layers, two factors were observed simultaneously first formation of the top layers rich in phosphorus and rhenium and decrease in Ni concentration within in the $(Cu,Ni)_6Sn_5$ phase when P concentration increased within coating. Concertation of Ni within $(Cu,Ni)_6Sn_5$ for finishing layers containing 4.0 wt.% Re was lower compared to the reference Ni-P samples, which indicate enhanced Ni diffusion blocking mechanism throw top layer by accumulated rhenium. The coexistence of the $(Cu,Ni)_6Sn_5$ and $(Ni,Cu)_3Sn_4$ phases at the interface of Ni/SAC has been the subject of several studies [22,23]. The $(Cu,Ni)_6Sn_5$ and $(Ni,Cu)_3Sn_4$ phases can crystallize simultaneously or individually, and their distribution at the phase boundary depends on experimental conditions, including the reaction time of the substrate with SAC305 solder. Preferential growth of the $(Ni,Cu)_3Sn_4$ phase, which serves as a heterogeneous growth site for the $(Cu,Ni)_6Sn_5$ phase, is suspected [22, 23]. Yang et al. [23] observed the growth of the $(Ni,Cu)_3Sn_4$ phase between the scallops of the $(Cu,Ni)_6Sn_5$ phase. In the present study, a continuous layer with a lighter SEM/BSE contrast (Fig. 5b-d and 6b-d), intersecting the $(Cu,Ni)_6Sn_5$ phase scallops, was identified by SEM/EDS as $(Ni,Cu)_3Sn_4$. Similar to Yang et al. [23] study that layer, in the form of fine needles, also filled the spaces between the $(Cu,Ni)_6Sn_5$ phase scallops. In these areas, the SEM/BSE contrast was non-uniform, and chemical composition measurements by SEM/EDS indicated that it corresponded to both the $(Cu,Ni)_6Sn_5$ and $(Ni,Cu)_3Sn_4$ phases (Fig. 5e, TABLE 2, points 8 and 9); therefore, a thin foil prepared from the area marked by a rectangle in Fig. 5e was further analyzed using the TEM technique.

Fig. 7 shows TEM/EDS chemical composition maps revealing the distribution of Ni, Cu, P, Re, and Sn at the interface of NiPRe4.7/SAC305. Based on the collected images, accumulation of phosphorus and rhenium, as well as depletion of nickel, were confirmed in the approximately 2 μm wide surface finish zone directly adjacent to the SAC305 solder. On the solder side, an uneven distribution of elements was observed, particularly of nickel and copper, indicating the formation of various intermetallic phases in which these elements dominate. Detailed investigations using selected area diffraction patterns (SADP) presented in Fig. 8 allowed identification of the $(Ni,Cu)_3Sn_2$ phase within Ni-enriched grains (marked 1 and 4) and the $(Cu,Ni)_6Sn_5$ phase within Cu-enriched grains (marked 3) on the elemental distribution maps (Fig. 7). SADP also confirmed the presence of pure tin (marked 2) in regions corresponding exclusively to tin in Fig. 7. Additionally, the presence of the $(Ni,Cu)_3Sn_4$ phase (marked 5) was identified directly at the NiPRe4.7/SAC305 interface along Ni-P-$Re_{P,Re\text{-}rich}$ zone. The $(Ni,Cu)_3Sn_2$ and $(Ni,Cu)_3Sn_4$ phases were also identified by Wojewoda-Budka et al. [6] at the Ni-P-Re/Sn surface finish interface. The $(Cu,Ni)_6Sn_5$ phase was not detected in that study, indicating that its presence at the interface was directly related to the chemical composition of the solder (SAC305), rather than to copper diffusion toward the

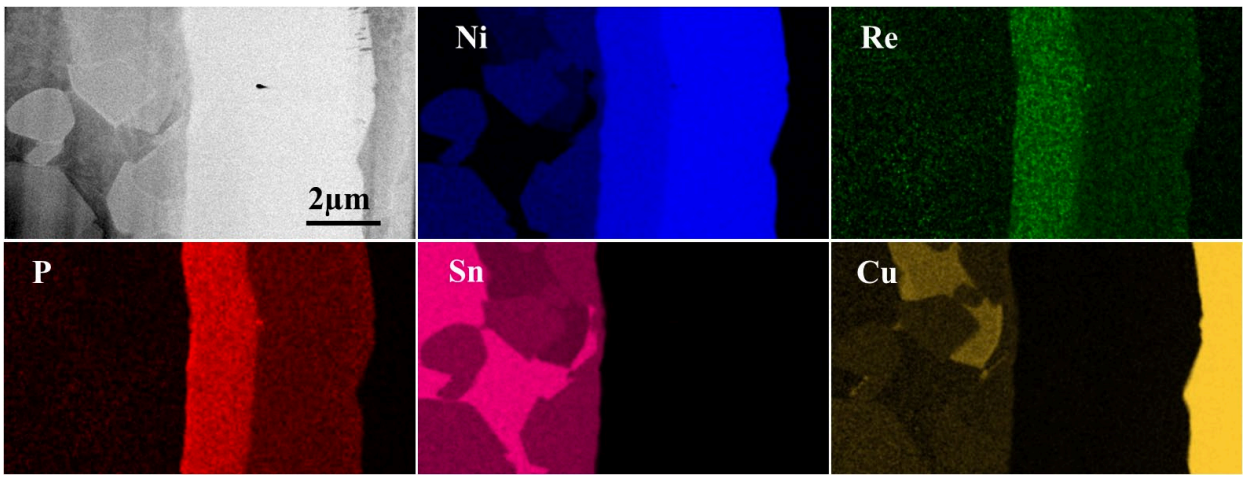

Fig. 7. TEM/STEM image of the NiPRe4.7/SAC305 interface with corresponding EDS maps showing the distribution of elements Ni, Cu, P, Re and Sn

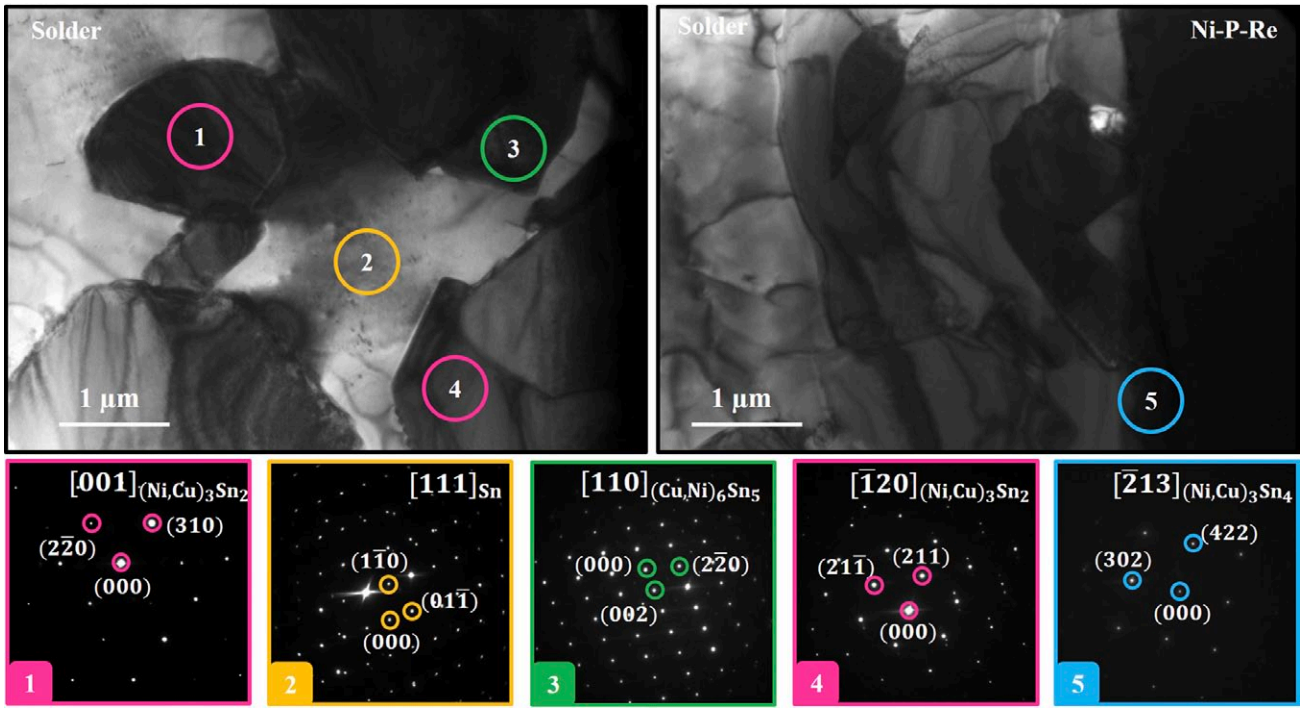

Fig. 8. Fig. TEM/BF image of the NiPRe4.7/SAC305 interface with the corresponding selected area diffraction patterns (SADP) from regions marked as 1-5

interface through the rhenium-enriched nickel-phosphorus coating. Moreover, such a phase distribution at the interface, in the area between the massive precipitates of the $(Cu,Ni)_6Sn_5$ phase (Fig. 5e), indicates the simultaneous formation of the $(Ni,Cu)_3Sn_2$ and $(Cu,Ni)_6Sn_5$ phases. The heterogeneous growth site for these phases is most likely the originally formed $(Ni,Cu)_3Sn_4$ phase located directly at the surface finish/SAC305 interface.

3.3. Thermal cycling of Ni-P and Ni-P-Re finishing layers with SAC305

Interface transformations in soldered joints made with lead-free Sn-Ag-Cu solders have been widely studied, particularly under isothermal aging conditions [24-26]. In the present study, thermal cycling was applied to simulate operating conditions in electronic systems and evaluate the effect of cyclic temperature variations on the formed interfaces. Fig. 9 presents a cross-sectional view through all interfaces after the heating and cooling cycles performed according to the temperature profile simulating thermal shocks during standard electronic device operation (Fig. 1). In most cases, no significant changes in the overall interface appearance occurred. In the solder volume, a reduced amount of loosely distributed precipitates of intermetallic phases detached from the interface was observed. At the interface of each sample, the presence of massive scallop-shaped $(Cu,Ni)_6Sn_5$ phases was observed. In the case of the Ni-P3.8 sample, the surface finish region identified as Ni-$P_{P\text{-}rich}$ after the wetting test (TABLE 2) was divided into two parts: Ni-$P_{P\text{-}rich}$ on the substrate side and Ni-P + Cu on the solder side. This indicates suppressed Cu diffusion from the substrate and, instead, diffusion of Cu from the SAC solder into the coating. At the interface, Ni_2SnP and $(Cu,Ni)_6Sn_5$ phases were still observed. Prior to thermal shock testing, Ni_2SnP existed as a continuous layer, while after applied temperature profile occurred only locally along the interface. In the case of the Ni-P-Re3.6 sample, the previously dispersed layer composed of small $(Cu,Ni)_6Sn_6$ clusters (Fig. 5d) transformed into a thin continuous film consisting of a mixture of Ni, P, Cu, and Sn. This layer is marked in TABLE 3 as Ni-P + Cu (copper side) or Ni-P + $(Cu,Ni)_6Sn_5$ (solder side). Changes at Ni-P4.8 interface involved disappearance of $(Ni,Cu)_3Sn_4$ phase previously growing within $(Cu,Ni)_6Sn_5$ scallops and between them. Currently between large precipites of $(Cu,Ni)_6Sn_5$ thin layer of Ni_2SnP layer was identified (TABLE 3). For the Ni-P-Re4.7 sample, the phase sequence remained unchanged. Within the Ni-P-Re coating, on the solder side a relatively thick (~2 µm) P- and Re-rich layer was still observed, now exhibiting extensive regions with numerous voids. The presence of such a zone indicates ongoing diffusion processes, particularly Ni diffusion into the solder, and the associated Kirkendall Effect. The voids present in the nickel-depleted layer in the initial state (after the wetting test) were significantly enlarged, and that zone widened. The areas where voids occur are much larger below the $(Cu,Ni)_6Sn_5$ phase precipitates, within which smaller $(Ni,Cu)_3Sn_4$ phase precipitates occur. This may indicate that Ni escaping from the surface finish is consumed in their formation. Repeated thermal cycling according to the thermal profile (Fig. 1) did not significantly affect the chemical phase composition or sequence at the Ni-P5.6/SAC305 interface. In the case of an identical sample containing rhenium (Ni-P-Re5.5), the resolution limitations of SEM/EDS analysis did not allow for the

determination of the chemical composition of the thin, bright layer observed along the P-rich region of the Ni-P-Re coating. However, based on previous investigations of this region in other samples, the formation of $(Ni,Cu)_3Sn_4$ is suspected. The overall phase sequence at the interface remained unchanged. Such observation indicates slowed diffusion processes at Ni-P-Re5.5/SAC305 and strong potential for reliable solder joint performance.

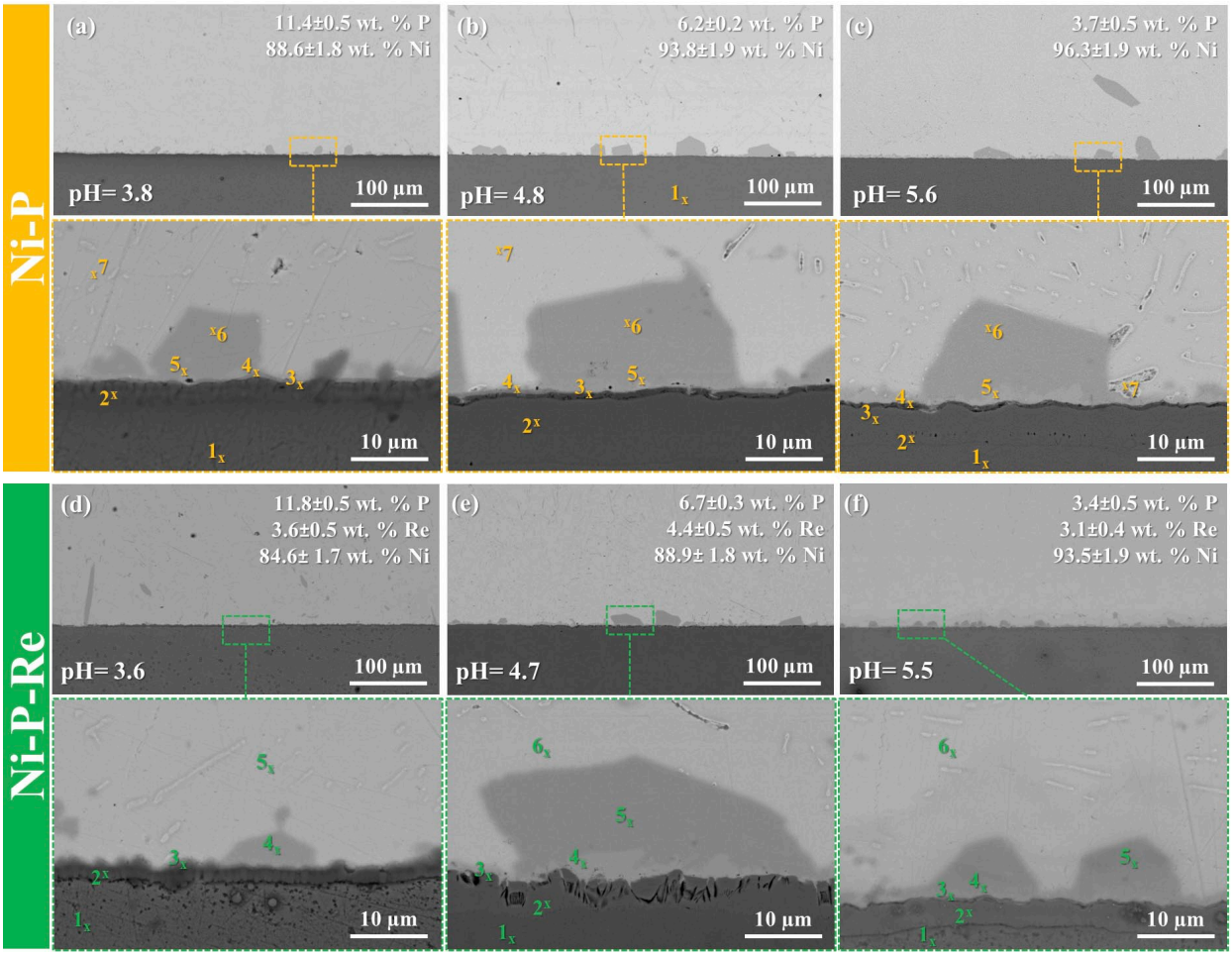

Fig. 9. SEM/BSE images of the interfacial cross-sections of Ni-P/SAC305 (a-c) and Ni-P-Re/SAC305 (d-f) after thermal cycling

TABLE 3

Average values of the SEM/EDS chemical composition collected from marked places of the cross sections Fig. 9a-f

Ni-P3.8 (Fig. 9a)																			
No	**Ni [at. %]**			**P [at. %]**			**Re [at. %]**			**Cu [at. %]**			**Sn [at. %]**			**Ag [at. %]**			**Possible Phase**
1		—			—			—		100.0	±	2.0		—			—		$Cu_{substrate}$
2	46.4	±	0.9	14.7	±	0.6		—		38.9	±	1.6		—			—		Cu + Ni-P
3	59.5	±	1.2	26.3	±	1.1		—		9.9	±	1.5	4.3	±	0.5		—		$Ni\text{-}P_{P\text{-}rich}$
4	50.9	±	7.6	20.3	±	0.5		—		5.5	±	0.6	23.3	±	0.5		—		Ni_2SnP
5	28.6	±	0.6	6.9	±	1.0		—		25.6	±	0.5	38.9	±	0.8		—		$(Cu,Ni)_6Sn_5$
6	20.4	±	0.5		—			—		35.3	±	0.7	44.3	±	0.9		—		$(Cu,Ni)_6Sn_5$
7		—			—			—			—		100.0	±	2.0		—		Sn
Ni-P4.8 (Fig. 9b)																			
No	**Ni [at. %]**			**P [at. %]**			**Re [at. %]**			**Cu [at. %]**			**Sn [at. %]**			**Ag [at. %]**			**Possible Phase**
1		—			—			—		100.0	±	2.0		—			—		$Cu_{substrate}$
2	91.8	±	1.8	8.2	±	0.8		—			—			—			—		Ni-P
3	79.5	±	1.6	19.2	±	0.8		—			—		1.3	±	0.6		—		$Ni\text{-}P_{P\text{-}rich}$
4	53.0	±	1.1	18.8	±	0.8		—		5.5	±	0.5	22.7	±	0.5		—		Ni_2SnP
5	34.1	±	0.7	6.8	±	1.0		—		24.4	±	1.0	34.7	±	0.7		—		$(Cu,Ni)_6Sn_5$
6	20.2	±	0.8		—			—		35.8	±	0.7	44.0	±	0.9		—		$(Cu,Ni)_6Sn_5$
7		—			—			—			—		100.0	±	2.0		—		Sn

TABLE 3. Continued

Ni-P5.6 (Fig. 9c)																			
No	**Ni [at. %]**			**P [at. %]**			**Re [at. %]**			**Cu [at. %]**			**Sn [at. %]**			**Ag [at. %]**			**Possible Phase**
1		—			—			—		100.0	±	2.0		—			—		$Cu_{substrate}$
2	93.4	±	1.9	6.6	±	1.0		—			—			—			—		Ni-P
3	91.0	±	1.8	9.0	±	0.5		—			—			—			—		$Ni\text{-}P_{P\text{-}rich}$
4	39.7	±	0.8		—			—		7.0	±	0.7	53.3	±	1.1		—		$(Ni,Cu)_3Sn_4$
5	21.4	±	0.9		—			—		34.4	±	0.7	44.2	±	0.9		—		$(Cu,Ni)_6Sn_5$
6		—			—			—			—		63.5	±	1.3	36.5	±	0.7	$Sn + Ag_3Sn$
7		—			—			—			—		100.0	±	2.0		—		Sn
Ni-P-Re3.6 (Fig. 9d)																			
No	**Ni [at. %]**			**P [at. %]**			**Re [at. %]**			**Cu [at. %]**			**Sn [at. %]**			**Ag [at. %]**			**Possible Phase**
1		—			—			—		100.0	±	2.0		—			—		$Cu_{substrate}$
2	24.2	±	0.5	12.2	±	1.8		—		54.4	±	2.2	9.2	±	0.5		—		Ni-P + Cu
3	20.9	±	0.5	7.0	±	0.3		—		35.9	±	1.4	36.2	±	1.4		—		$Ni\text{-}P + (Cu,Ni)_6Sn_5$
4	10.3	±	0.5		—			—		44.8	±	0.9	44.9	±	0.9		—		$(Cu,Ni)_6Sn_5$
5		—			—			—			—		100.0	±	2.0		—		Sn
Ni-P-Re4.7 (Fig. 9e)																			
No	**Ni [at. %]**			**P [at. %]**			**Re [at. %]**			**Cu [at. %]**			**Sn [at. %]**			**Ag[at. %]**			**Possible Phase**
1		—			—			—		100.0	±	2.0		—			—		$Cu_{substrate}$
2	88.0	±	1.8	10.9	±	0.5	1.1	±	0.5		—			—			—		Ni-P-Re
3	71.6	±	1.5	25.7	±	0.6	2.7	±	0.5		—			—			—		$Ni\text{-}P\text{-}Re_{P,Re\text{-}rich}$
4	37.4	±	0.5		—			—		8.8	±	0.5	53.8	±	1.4		—		$(Ni,Cu)_3Sn_4$
5	21.3	±	0.6		—			—		34.9	±	0.5	43.8	±	1.2		—		$(Cu,Ni)_6Sn_5$
6		—			—			—			—		100.0	±	2.0		—		Sn
Ni-P-Re5.5 (Fig. 9f)																			
No	**Ni [at. %]**			**P [at. %]**			**Re [at. %]**			**Cu [at. %]**			**Sn [at. %]**			**Ag [at. %]**			**Possible Phase**
1		—			—			—		100.0	±	2.0		—			—		$Cu_{substrate}$
2	94.2	±	1.9	5.8	±	0.6		—						—			—		Ni-P-Re
3	70.4	±	1.3	15.3	±	0.6		—		2.7	±	0.5	11.6	±	0.6		—		$Ni\text{-}P\text{-}Re_{P\text{-}rich}$
4	25.1	±	0.7					—		31.1	±	0.5	43.8	±	1.2		—		$(Cu,Ni)_6Sn_5$
5	19.6	±	0.5		—			—		37.2	±	0.5	43.2	±	1.2		—		$(Cu,Ni)_6Sn_5$
6		—			—			—		100.0	±	2.0		—			—		Sn

4. Conclusions

- The experimental procedure enabled the deposition of matte, silver-colored finishing layers free of defects, exhibiting morphology typical of electroless nickel.
- The application of varying concentrations of ammonium perrhenate, along with slight adjustments of the initial pH (by 0.1-0.2 units compared to the baseline conditions), allowed for the deposition of Ni-P-Re finishing layers with a nearly constant rhenium content and a phosphorus content comparable to reference Ni-P series. Rhenium was co-deposited into the finishing layers at the expense of nickel.
- The series of Ni-P-Re samples exhibited better wettability by SAC305 solder than the reference Ni-P samples. The highest wettability was observed for the Ni-P-Re5.5 coating, while the lowest was recognized for Ni-P4.8. For the Ni-P series, no clear trend of increasing wettability with decreasing phosphorus content was observed. In contrast, for the Ni-P-Re finishing layers, despite similar changes in surface roughness, wettability by SAC305 increased with decreasing phosphorus content.
- A higher phosphorus content in the finishing layers promotes the massive detachment of intermetallic compounds from the interface, and the chemical composition of the spalled particles corresponds to that of the $(Cu,Ni)_6Sn_5$ scallops formed along the entire interface. Therefore, it can be concluded that this phase does not form spontaneously within the solder as a result of its chemical composition during solidification of the droplet.
- The formation of the unfavorable Ni_2SnP phase along the interface, leading to an intense spalling effect, was observed only for high-phosphorus Ni-P finishing layers. A decrease in phosphorus content suppressed the formation of Ni_2SnP, while $(Ni,Cu)_3Sn_4$ was identified within the $(Cu,Ni)_6Sn_5$ phase. A needle-shaped layer located between the $(Cu,Ni)_6Sn_5$ phases was identified as a mixture of $(Ni,Cu)_3Sn_4$, Sn, $(Cu,Ni)_6Sn_5$, and $(Ni,Cu)_3Sn_2$. Due to its location directly adjacent to the surface finish interface and its small thickness, the $(Ni,Cu)_3Sn_4$ phase is considered to act as a heterogeneous nucleation site for the growth of the $(Cu,Ni)_6Sn_5$ phase.
- The interfacial region of the surface finish is depleted in Ni due to its diffusion into the solder, while P and Re accumulate in this zone, and the underlying surface finish retains its original composition. This segregation, together with increasing P content and reduced Ni concentration in

the $(Cu,Ni)_6Sn_5$ phase, indicates that alloying additions suppress Ni diffusion toward the solder, thereby enhancing interfacial stability.

- Thermal cycling had a limited effect on the phase sequence but induced diffusion-driven changes, including Ni depletion correlated with void formation within the coating, reduced spalling, and redistribution of the Ni_2SnP phase.
- The Ni-P-Re5.5/SAC305 system exhibited the highest interfacial stability, showing no changes in phase sequence, no void formation, and no significant spalling after thermal cycling, indicating slowed diffusion processes and strong potential for reliable solder joint performance.

Acknowledgements

The research was financially supported by the National Science Centre, Poland, under the Miniatura 8 project No. 2024/08/X/ST11/01768.
Wettability tests were conducted as part of a cooperation agreement signed between Joanna Wojewoda-Budka representing IMMS PAS and Fabrizio Valenza representing ICMATE CNR.

REFERENCES

[1] K. Bukat, H. Hackiewicz, Lutowanie bezołowiowe, Wydawnictwo BTC (2007).

[2] E.E. Noor, N.F. Nasir, S.R.A. Idris, A review: lead free solder and its wettability properties. Solder Surf. Mt. Technol. **28** (3), 125-132 (2016). DOI: https://doi.org/10.1108/ssmt-08-2015-0022

[3] M. Sobolewski, J. Wojewoda-Budka, N. Sobczak, M. Janusz-Skuza, A. Bigos, S. Terlicka, A. Korneva, M. Szlezynger, Z. Adamek, A. Wierzbicka-Miernik, Green electronics soldering by application of third generation lead-free solder alloys: studies on their wettability and interface microstructure formed with copper. J. Mater. Eng. Perform. **34**, 28134-28144 (2025).
DOI: https://doi.org/10.1007/s11665-025-12029-0

[4] A. Bigos, F. Valenza, P. Czaja, I. Kwiecień, J. Wojewoda-Budka, Interface reaction between tin solder and nanocrystalline Ni and Ni-Mo coatings obtained by electrodeposition. J. Mater. Eng. Perform. **31**, 7061-7067 (2022).
DOI: https://doi.org/10.1007/S11665-022-06840-2

[5] A. Bigos, M. Janusz-Skuza, F. Valenza, S. Gambaro, J. Wojewoda-Budka, Influence of molybdenum on wetting and interfacial reactivity of Ni-Mo coatings with Sn and Sn-3.5 wt.% Ag-0.5 wt.% Cu solders. Surf. Interfaces **86**, 108749 (2026).
DOI: https://doi.org/10.1016/j.surfin.2026.108749

[6] J. Wojewoda-Budka, A. Wierzbicka-Miernik, I. Kwiecień, F. Valenza, A. Korneva, M. Janusz-Skuza, K. Stan-Głowińska, J. Guspiel, M. Bugajska, Reactivity with tin and corrosion resistance of electroless Ni-P and Ni-P-Re coatings plated on copper. Electrochim. Acta **406**, 139850 (2022).
DOI: https://doi.org/10.1016/j.electacta.2022.139850

[7] I. Kwiecien, M. Bugajska, M. Janusz-Skuza, A. Bigos, F. Valenza, A. Wierzbicka-Miernik, A. Larrañaga Varga, G.A. Lopez, J. Wojewoda-Budka, High phosphorus electroless NiP coatings – effect of rhenium addition on coating/solder interface. Surf. Interfaces **56**, 105548 (2025).
DOI: https://doi.org/10.1016/j.surfin.2024.105548

[8] Z.L. Ma, S.A. Belyakov, C.M. Gourlay, Effects of cobalt on the nucleation and grain refinement of Sn-3Ag-0.5Cu solders. J. Alloys Compd. **682**, 326-337 (2016).
DOI: https://doi.org/10.1016/j.jallcom.2016.04.265

[9] J. Xing, J. Yao, Y. Zhao, et al., The feasibility study of replacing the traditional amorphous Ni-P with an amorphous Ni-Cu-P layer. J. Mater. Sci.: Mater. Electron. **35**, 833 (2024).
DOI: https://doi.org/10.1007/s10854-024-12457-z

[10] K.N. Subramanian, Lead-free electronic solders, Springer, New York, USA (2007).

[11] J. Wang, S. Xue, P. Zhang, P. Zhai, Y. Tao, The reliability of lead-free solder joint subjected to special environment: a review. J. Mater. Sci.: Mater. Electron. **30**, 9065-9086 (2019).
DOI: https://doi.org/10.1007/s10854-019-01333-w

[12] Y. Yang, J.N. Balaraju, S.C. Chong, H. Xu, C. Liu, V.V. Silberschmidt, Z. Chen, Significantly retarded interfacial reaction between an electroless Ni–W–P metallization and lead-free Sn–3.5Ag solder. J. Alloys Compd. **15**, 11-16 (2013).
DOI: https://doi.org/10.1016/j.jallcom.2013.02.113

[13] Y. Yang, J.N. Balaraju, Y. Huang, H. Liu, Z. Chen, Interface reaction between an electroless Ni–Co–P metallization and Sn–3.5Ag lead-free solder with improved joint reliability. Acta Mater. **71**, 69-79 (2014).
DOI: https://doi.org/10.1016/j.actamat.2014.02.026

[14] S. Gambaro, F. Valenza, M.L. Muolo, A. Passerone, G. Cacciamani, Wettability of SiC and graphite by Co–Ta alloys: evaluation of the reactivity supported by thermodynamic calculations. J. Mater. Sci. **52**, (2017).
DOI: https://doi.org/10.1007/s10853-017-1448-0

[15] W. Sha, X. Wu, K.G. Keong, Electroless copper and nickel-phosphorus plating: processing, characterisation and modelling, Elsevier (2011).
DOI: https://doi.org/10.1533/9780857090966

[16] H. Kazimierczak, A. Wierzbicka-Miernik, I. Kwiecień, M.J. Szczerba, A. Korneva, M. Mosiałek, K. Miernik, J. Wojewoda-Budka, Electroless deposition of Ni–P and Ni–P–Re alloys from acidic hypophosphite baths. Electrochim. Acta **303**, (2019).
DOI: https://doi.org/10.1016/j.electacta.2019.02.057

[17] J. Wojewoda-Budka, A. Wierzbicka-Miernik, M. Szczerba, H. Kazimierczak, I. Kwiecień, J. Morgiel, K. Stan-Głowińska, F. Valenza, The effect of Re addition on the thermal stability and structure of Ni-P electroless coatings. Mater. Charact. **171**, 110811 (2021).
DOI: https://doi.org/10.1016/j.matchar.2020.110811

[18] J. Wojewoda-Budka, Z. Huber, L. Lityńska-Dobrzyńska, N. Sobczak, P. Zięba, Microstructure and chemistry of the SAC/ENIG interconnections. Mater. Chem. Phys. **139**, 276-280 (2013).
DOI: https://doi.org/10.1016/j.matchemphys.2013.01.035

[19] Y.C. Lin, K.J. Wang, J.G. Duh, Detailed phase evolution of a phosphorous-rich layer and formation of the Ni-Sn-P compound in Sn-Ag-Cu/electroplated Ni-P solder joints. J. Electron. Mater. **39**, 283-294 (2010).
DOI: https://doi.org/10.1007/s11664-009-1014-x

[20] Y.C. Sohn, J. Yu, S.K. Kang, W.K. Choi, D.Y. Shih, Study of the reaction mechanism between electroless Ni-P and Sn and its effect on the crystallization of Ni-P. J. Mater. Res. **18**, 4-7 (2003).
DOI: https://doi.org/10.1557/jmr.2003.0002

[21] J.W. Yoon, S.W. Kim, S.B. Jung, Effect of reflow time on interfacial reaction and shear strength of Sn–0.7Cu solder/Cu and electroless Ni–P BGA joints. J. Alloys Compd. **385**, 192-198 (2004). DOI: https://doi.org/10.1016/j.jallcom.2004.05.009

[22] C.E. Ho, R.Y. Tsai, Y.L. Lin, C.R. Kao, Effect of Cu concentration on the reactions between Sn-Ag-Cu solders and Ni. J. Electron. Mater. **31** (6), 584-590 (2002).
DOI: https://doi.org/10.1007/s11664-002-0129-0

[23] J. Yang, P. Shen, Z. Yin, J. Sun, Q. Jiang, Wetting of microcrystalline and nanocrystalline Ni substrates by molten Sn-3.5Ag-0.7Cu alloy. Mater. Lett. **64**, 2454-2457 (2010).
DOI: https://doi.org/10.1016/j.matlet.2010.08.017

[24] A.R. Fix, G.A. López, I. Brauer, W. Nüchter, E.J. Mittemeijer, Microstructural development of Sn–Ag–Cu solder joints. J. Electron. Mater. **34**, 137-142 (2005).
DOI: https://doi.org/10.1007/s11664-005-0224-0

[25] J.W. Yoon, S.B. Jung, Effect of surface finish on interfacial reactions of Cu/Sn–Ag–Cu/Cu(ENIG) sandwich solder joints. J. Alloys Compd. **448**, 177-184 (2008).
DOI: https://doi.org/10.1016/j.jallcom.2006.10.052

[26] W. Seo, M.-S. Kim, Y.-H. Ko, Y.-H. Kim, S. Yoo, Growth of intermetallic compounds and brittle fracture behavior of Sn–Ag–Cu/ENIG joint with columnar Ni–P layer. J. Mater. Sci.: Mater. Electron. **32**, 1042-1051 (2021).
DOI: https://doi.org/10.1007/s10854-020-04879-2